Microscopic calculations of potential energy surfaces: fission and fusion properties

L. Bonneau[*] and P. Quentin[†,*]

[*]*Los Alamos National Laboratory, Theoretical Division, MS B283, Los Alamos, New Mexico 87545 USA*
[†]*Centre d'Etudes Nucléaires de Bordeaux-Gradignan, CNRS-IN2P3 and Université Bordeaux I, BP 120, 33175 Gradignan, France*

Abstract.
Various valleys of the deformation potential energy surface relevant to fission and fusion processes have been investigated within the same Skyrme–Hartree–Fock plus BCS microscopic model in the $A = 70$ and $A > 220$ mass regions. The available experimental fission barrier heights of actinides are reproduced within a rms error of 1.5 MeV whereas the conditional barriers of the considered light nucleus are overestimated by about 10 MeV. The fission paths describing the descent from saddle to scission have been found consistent with the results obtained with the Gogny force used in the Hartree–Fock–Bogolyubov approach and in agreement with the experimental mass distributions. In general, the valleys corresponding to very asymmetric separated shapes (close to the Pb plus light partner configuration) are in agreement with the most favorable target-projectile combinations in cold fusion reactions experimentally used to form such compound nuclei. The deduced fusion barrier heights have been found about 10 MeV lower than those obtained within the Extended Thomas Fermi model.

Keywords: self-consitent microscopic approach, potential energy surface, fission barrier, most probable fragmentation, fusion barrier
PACS: 21.60.Jz, 24.75.+i, 25.70.-z

1. INTRODUCTION

The nuclear fission process constitutes a remarkable challenge for any theory, especially for a microscopic one. A large amplitude collective motion as well as nuclear configurations far from the ground state (GS) equilibrium solution are involved: both dynamic and static properties thus play significant roles. The same can also be said about the reverse process, namely the fusion of colliding heavy ions. From the static standpoint, these processes are both governed by the topology of the potential energy surface (PES) of the considered compound nucleus (CN), especially when the excitation energy of the latter with respect to its GS is low.

In this respect, we aim at investigating the PES of various nuclei with a view to extracting low energy fission and fusion static properties at once. In this perspective, we have applied earlier the self-consistent mean field Skyrme–Hartree–Fock plus BCS model to the study of fission barriers in the actinide region [1] and very recently, we have extended it to the $A = 70$ mass region (below the Businaro–Gallone point), taking the example of the ^{70}Se isotope [2]. The compilation of the obtained barrier heights is presented in Sect. 2 together with new results for three additional actinides. Then we have investigated the various fission paths leading from the outer saddle point to

separated fragments configurations. The results and their consequences in terms of fragment mass and kinetic energy distributions are discussed in Sect. 3. Finally we have shown in various mass regions that the potential energy surface possesses several fusion valleys with high mass asymmetry, from which we have deduced fusion barrier heights. This is discussed and compared to other calculations and experimental data in Sect. 4.

2. FISSION BARRIERS

In a previous paper [1], the above mentioned model has been decribed and applied to the calculation of fission barriers for twenty-six actinides among which six could be compared with available experimental data, namely the ^{230,232}Th, ^{234,236}U, ^{240}Pu and ^{252}Cf isotopes. Their barrier heights and those of three additional actinides (^{228}Ra, ^{226}Th and ^{238}U) are reported in Tab. 1. They differ on average by about 1.5 MeV (rms error) from the experimental values. It is worth reminding here that the latter are extracted from fission cross-section data assuming a double-humped, parabolic shape of the barriers. They include many-dimension effects in the effective, one-dimension barrier parameters. Instead, the theoretical values are obtained by exploring a restricted deformation space, the other degrees of freedom taking their values giving a local minimum (not necessarily the lowest a priori) in the full potential energy surface. As can be seen on the left panel of Fig. 1, the barrier profiles can be far from looking parabolic. Finally, one has also to bear in mind that the pairing strength entering the present model has been kept fixed for all the studied nuclei and has not been adjusted to reproduce such deformation properties.

TABLE 1. Inner (E_A) and outer (E_B) fission barrier heights for nine actinides (left values) compared with experimental data (right values) from Ref. [3] (from Ref. [4] for ^{252}Cf).

Nucleus	E_A (MeV)		E_B (MeV)	
^{228}Ra	5.3	8.0±0.5	6.0	8.5±0.5
^{226}Th*	6.4	5.9±0.3	6.5	6.6±0.3
^{230}Th	4.9	6.1±0.2	4.4	6.5±0.3
^{232}Th	5.5	5.8±0.2	4.1	6.2±0.2
^{234}U	5.3	5.6±0.2	5.1	5.5±0.2
^{236}U	6.2	5.6±0.2	4.6	5.5±0.2
^{238}U	7.3	5.7±0.2	4.4	5.7±0.2
^{240}Pu	7.1	5.6±0.2	4.1	5.1±0.2
^{252}Cf	7.1	5.3	2.9	3.5

* experimental values for ^{227}Th

Very recently, we have applied the same model (with a different pairing strength, though) to the lightest nucleus for which experimental data are currently available, namely the ^{70}Se isotope [2]. This nucleus lies below the Businaro–Gallone point and is slightly neutron-deficient, which makes challenging the task of calculating conditional fission barriers in this mass region. We have found two shallow local minima close to the spherical point, one being prolate, the other one oblate (the lower among both). Starting from the spherical point we have determined the path leading to fission, called ground state ascending valley (full line in the right panel of Fig. 1), and we have shown

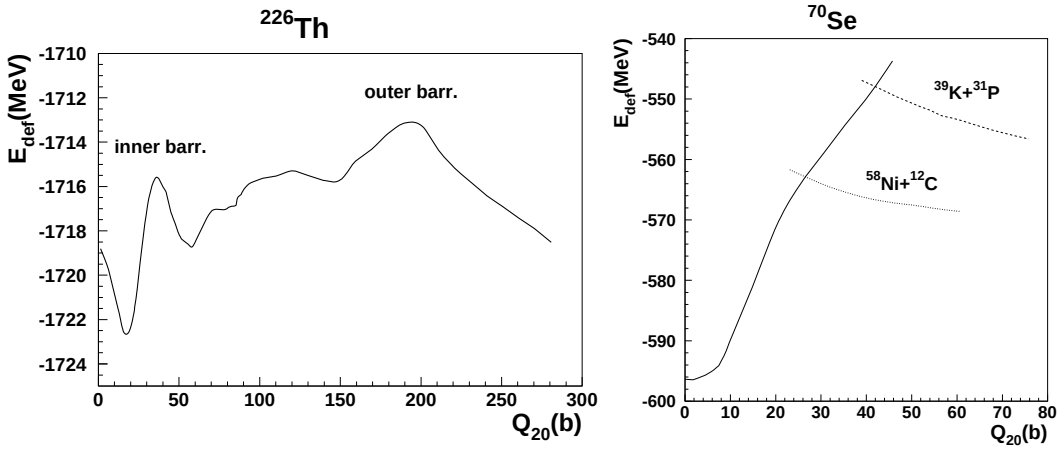

FIGURE 1. Left panel: deformation energy (in MeV) along the fission barrier of the ^{226}Th isotope as a function of the total axial quadrupole moment Q_{20} (in barns). Right panel: deformation energy along the fission and fusion valleys of ^{70}Se as a function of Q_{20}.

that it is stable against left-right asymmetric as well as triaxial distortions. We have also found two fusion valleys corresponding to two different fragmentations, namely ^{58}Ni+^{12}C and ^{39}K+^{31}P (dotted and dashed line in Fig. 1, respectively). We have then sought for a continuous path connecting the GS ascending valley to each of these exit channels. For a given exit channel, the highest point along the corresponding path gives a priori only an upper limit of the conditional fission barrier height. To obtain the actual value of the latter, it is necessary to explore the entire PES restricted to the most relevant shape coordinates, for example in a similar way as the calculations by P. Möller and collaborators in five dimensions (see, e.g., Ref. [5]). This is a very demanding task which is nowadays out of reach of any Hartree–Fock type calculations, essentially for computation time reasons. In Tab. 2 we have reported our theoretical values, compared to the experimental values of T. S. Fan and collaborators [6]. As can be noticed, our

TABLE 2. Conditional fission barriers for the ^{70}Se nucleus compared with experimental data taken from Ref. [6].

Z_{light}	SHF+BCS [2]	exp.
6	34.7	25.3±0.8
15	44.9	35.1±0.8

barrier heights overestimate by almost 10 MeV the experimental ones. To put this result in the proper perspective, in addition to the upper limit character of our values, it is also worth recalling that it was, before this work, commonly thought that our overestimation should be much larger on the basis of a semi-classical estimate of the curvature liquid drop energy, which relies on the leptodermous approximation for the nuclear density [7]. The latter might no longer be valid for saddle point shapes close to scission point shapes, as it is the case for such light nuclei as ^{70}Se.

3. FISSION PATHS AND MOST PROBABLE FRAGMENTATIONS

Beyond the outer saddle point we have determined several fission paths leading to separated fragments configurations. To do so we have let the degrees of freedom other than the elongation Q_{20} (essentially the mass asymmetry Q_{30} and the neck coordinate Q_N) take the values minimizing the deformation energy of the CN. We have searched for several possible such local minima by varying the starting point of the iterative Hartree–Fock process. This has led to the various valleys displayed in Figs. 2, 3 and 4 for six

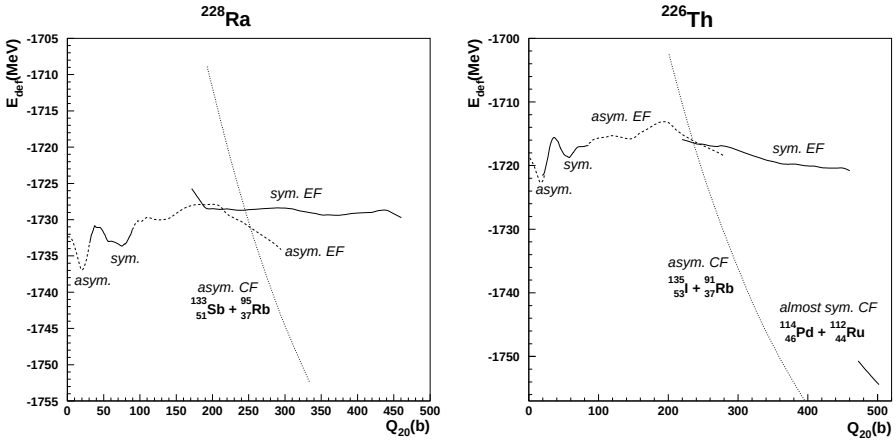

FIGURE 2. Fission and fusion valleys of the ^{228}Ra and ^{226}Th isotopes. Left-right symmetric solutions are displayed in full line, whereas the asymmetric ones appear as dashed lines. The dotted lines represent two-fragments solutions, regardless of their symmetric or asymmetric character.

actinides: ^{228}Ra, ^{226}Th, ^{238}U, ^{252}Cf, ^{256}Fm and ^{258}Fm.

The first two of these isotopes exhibit similar PES patterns. First their GS shape is found to be left-right asymmetric. Moreover two valleys corresponding to one-body shaped, elongated configurations develop around and beyond the outer saddle point: one for left-right asymmetric solutions called asymmetric elongated fission path, the other one for symmetric solutions called symmetric elongated fission path. They are labeled “asym. EF” and “sym. EF” in Fig. 2, respectively. In the same elongation range, we have found a valley called asymmetric compact fission path and labeled “asym. CF” in Fig. 2 describing two-fragments solutions. Whereas the asymmetric EF valley is continuously connected to the GS, the symmetric EF valley is separated from the former by a ridge. From this topological features we can infer that the very low energy fission (up to about 10 MeV) of these two isotopes would preferably proceed through the asymmetric path, leading to an asymmetric fragmentation with a mass ratio $A_H/A_L \approx 133/95$ (heavy fragment mass over light fragment mass) for ^{228}Ra and a charge ratio $Z_H/Z_L \approx 53/37$ for ^{226}Th. These values are consistent with the experimental peak-to-peak ratios for the mass distribution of ^{228}Ra (of about 136/92) [8] and for the element distribution of ^{226}Th (amounting to 54/36) [9]. At higher energy, in addition to the previous asymmetric path, the symmetric EF one becomes energetically accessible, which opens the symmetric division channel. This is in qualitative agreement with the experimental observation of three-peak fragment mass and element distributions for the neutron- and electromagnetic-induced fission of ^{228}Ra [8] and ^{226}Th [9], respectively.

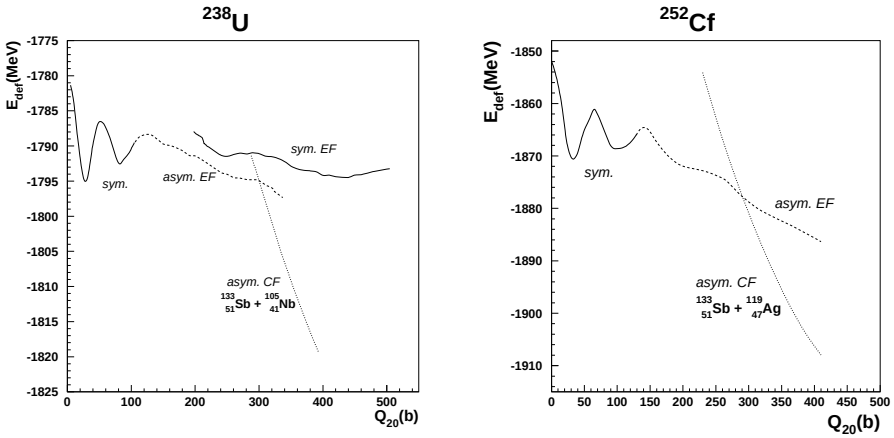

FIGURE 3. Same as Fig. 2 for the ^{238}U and ^{252}Cf isotopes.

As for the ^{238}U isotope (left panel of Fig. 3), we have obtained similar valleys. However the symmetric EF valley is found to lie between 2.5 MeV and 5 MeV above the asymmetric EF one all along the Q_{20} range where they coexist, which makes it virtually inaccessible in low energy fission. As a result, the most favorable path towards fission is the asymmetric one, ending with a fragmentation whose calculated mass ratio ($\approx$133/105) is somewhat lower than the peak-to-peak ratio (about 142/96) for the experimental mass distribution of ^{238}U spontaneous fission [10]. In the case of ^{252}Cf, only an asymmetric path has been found, leading to a mass ratio $A_H/A_L \approx 133/119$ also underestimating the experimental value (143/109) [11]. It is interesting to note that similar valleys have been obtained for ^{252}Cf by M. Warda and collaborators in the Hartree–Fock–Bogolyubov approach using the D1S Gogny interaction [12]. In particular, these authors have found almost the same mass ratio $A_H/A_L \approx 134/118$.

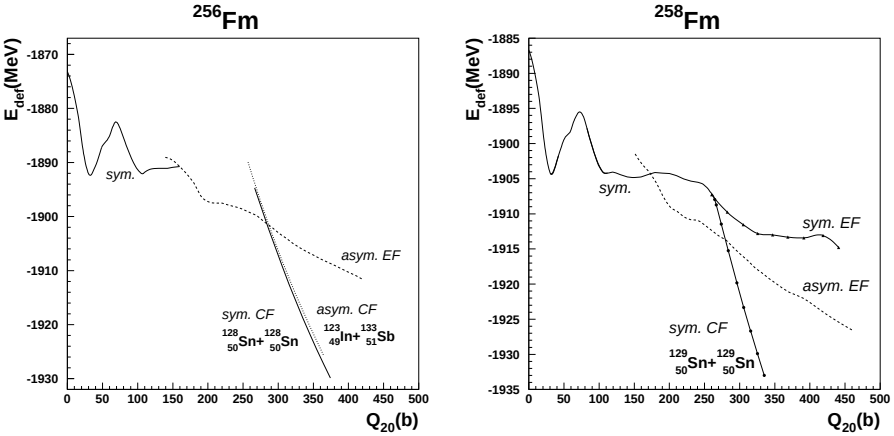

FIGURE 4. Same as Fig. 2 for the ^{256}Fm and ^{258}Fm isotopes.

Finally, the case of the ^{256,258}Fm isotopes is of particular interest since they exhibit totally different fragment mass distribution patterns (for spontaneous fission): whereas the ^{256}Fm nucleus has a broad, asymmetric mass distribution [13], that of the ^{258}Fm is

symmetric, sharply peaked at $A = 129$ [14]. On the one hand, only an asymmetric path has been found for the ^{256}Fm isotope (dashed line in the left panel of Fig. 4), eventually falling down into an asymmetric fusion valley (dotted line). It is interesting to note that a symmetric fusion valley has been also obtained, separated from the latter by a ridge (of about 1-2 MeV in the upper part of the valleys). On the other hand, the predominant path that has been found in the ^{258}Fm case turns out to be symmetric. It remarkably connects the GS to the (symmetric) fusion valley (solid line with full circles) in a continuous way. Correlatively, the asymmetric fission valley also present in the PES of ^{258}Fm is separated from the symmetric paths by a ridge, making it much less accessible. Another interesting feature is the existence of a second symmetric valley (EF path represented as a solid line with full triangles in Fig. 4). Whereas the two fragments are formed very close to each other at the early stages of the CF path, leading to a high TKE mode, the much larger center of mass distance between fragments at the very end of the EF path is responsible for a lower TKE mode. This could explain the experimentally well known bimodal fission of ^{258}Fm [15], in contrast to the explanation of M. Warda and co-authors in Ref. [16] invoking the asymmetric EF path to account for the low TKE mode.

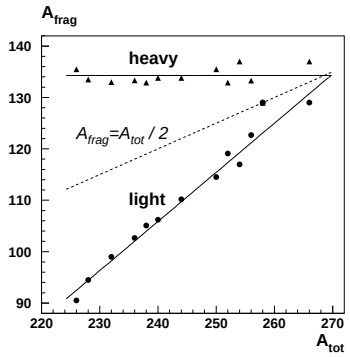

FIGURE 5. Most probable heavy and light fragments masses as a function of compound system mass.

In view of the preceding discussion, the obtained fusion valleys (two-fragments configurations) correspond to the most probable fragmentations. They are due to shell effects in the heavy fragment, close to the doubly-magic ^{132}Sn. As shown in Fig. 5 for the above presented actinides and several additional ones (as well as for the ^{266}Hs superheavy nucleus whose main valleys are displayed in Fig. 6 and discussed in Sect. 4), the heavy fragment mass is rather constant as the CN mass increases. This behaviour is consistent with microscopic-macroscopic calculations [17] and with the similar trend experimentally observed for the mean heavy fragment mass (see Fig. 4 of Ref. [13]).

4. FUSION BARRIERS

In addition to the above discussed fusion valleys corresponding to the $N = 82$ and $Z = 50$ shell effects in the heavy fragment, we have also found one valley corresponding to the $N = 50$ shell effect in the light fragment and another one where the heavy partner is close to the doubly-magic ^{208}Pb (refered here as to the hyper-asymmetric (HA) fusion valley). In Fig. 6 we have displayed all the fusion valleys found for three very heavy nuclei

(^{256}Fm, ^{258}Fm and ^{266}Hs). In fact the HA fusion valley can be interpreted as the most energetically favored target+projectile combination in a cold fusion reaction forming the considered CN. The deduced fusion barrier height $B_{fus}^{(HF)}$, defined as the difference

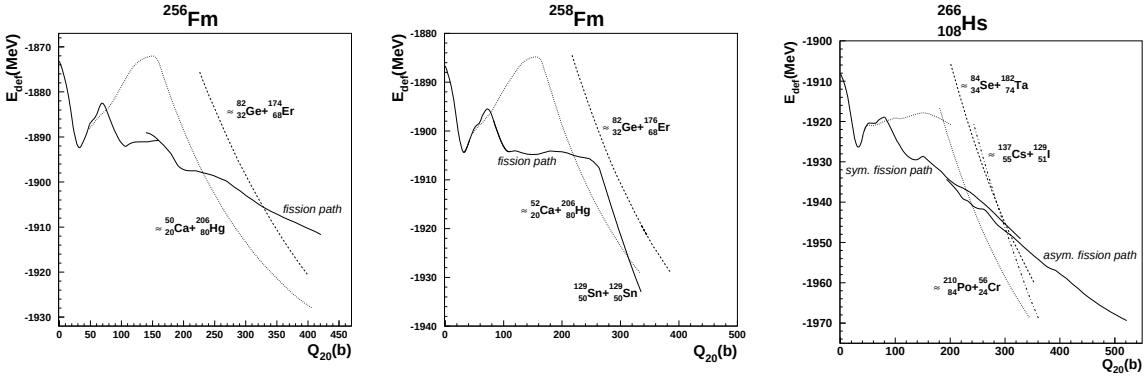

FIGURE 6. Fusion and fission valleys of the compound nuclei ^{256}Fm, ^{258}Fm and ^{266}Hs.

between the energy at the top of the fusion valley and the sum of the projectile and target GS energies, is reported in Tab. 3 for each of these 3 nuclei together with the theoretical values obtained in three other models: the microscopic-macroscopic model [18], the Extended Thomas Fermi model [19] and the Bass model with the parameters of Ref. [20]. In the present work, $B_{fus}^{(HF)}$ is actually calculated as

$$B_{fus}^{(HF)} = E_{CN}^{(min)} + Q_{\rm fis}\,,$$

where $E_{CN}^{(min)}$ is the height of the fusion barrier with respect to the GS of the CN (i.e, the minimal excitation energy at which the CN is formed just at the top of the fusion barrier) and $Q_{\rm fis}$ is the Q-value corresponding to the fission of the considered CN into the target+projectile fragmentation (for which we have used the experimental value). On the

TABLE 3. Fusion barrier heights and minimal CN excitation energies (with respect to the GS of the CN) compared with other theoretical results and with the experimental value [21], respectively.

CN	reaction	$E_{CN}^{(min)}(exp)$	$E_{CN}^{(min)}(HF)$	$B_{fus}^{(HF)}$	$B_{fus}^{(mic-mac)}$	$B_{fus}^{(ETF)}$	$B_{fus}^{(Bass)}$
^{256}Fm	^{206}Hg+^{50}Ca		20.0	166.3		175.5	
^{258}Fm	^{206}Hg+^{52}Ca		19.5	163.3		174.7	
^{266}Hs	^{212}Po+^{56}Cr		9.7	202.1		219.8	
^{266}Hs	^{208}Pb+^{58}Fe	$\sim$10			221.96	232.5	226.8

experimental side, the ^{266}Hs CN has been formed by the ^{208}Pb(^{58}Fe,1n)^{265}Hs reaction and the corresponding excitation function has been measured by S. Hoffman and collaborators [21]. Our most favorable target+projectile combination ^{212}Po+^{56}Cr being very close to the one experimentally used, we have also included the experimental $E_{CN}^{(min)}$-value in Tab. 3. The latter is the minimal energy above which the excitation function takes appreciable values. Whereas we underestimate the other theoretical barrier heights by 10 to 20 MeV, our $E_{CN}^{(min)}$-value is close to the experimental one, which might indicate that the deformations of *both* fragments have to be taken into account.

5. CONCLUSION AND PERSPECTIVES

We have shown that we can learn more about the fission and fusion properties from the static study of the PES in the Skyrme–Hartree–Fock plus BCS approach. The obtained results generally agree with the experimental data and are consistent in most cases with the calculations in the Hartree–Fock–Bogolyubov and microscopic-macroscopic models. However, the constant pairing interaction (so-called seniority force) does not seem to be appropriate for two-fragments shapes. A δ-interaction for example would better describe the pairing correlations separately in both fragments. Moreover, a particle number conserving approach should rather be used instead of the BCS or Bogolyubov approximations, especially when one is interested in properties varying rapidly with the nucleon number (like the shape transition of the mass distribution in the Fm isotopic chain). Finally, the center of mass correction (performed here upon using a one-body operator approximation) should require a better treatment around and beyond the scission point.

ACKNOWLEDGMENTS

We are grateful to A. J. Sierk and P. Möller for fruitful discussions. One of the authors (Ph. Q.) thanks the Theoretical Division at LANL for the excellent working conditions extended to him during numerous visits. This work has been supported by the U.S. Department of Energy under contract W-7405-ENG-36.

REFERENCES

1. L. Bonneau, P. Quentin and D. Samsœn, *Eur. Phys. J. A* 21, 391 (2004)
2. L. Bonneau and P. Quentin, submitted to *Phys. Rev. C*
3. S. Bjørnholm and J. E. Lynn, *Rev. Mod. Phys.* 52, 725 (1980)
4. G. N. Smirenkin, *IAEA Report*, INDC(CCP)-359 (1993)
5. P. Möller, A. J. Sierk and A. Iwamoto, *Phys. Rev. Lett.* 92, 072501 (2004).
6. T. S. Fan et al., *Nucl. Phys. A* 679, 121 (2000).
7. W. Stocker, J. Bartel, J. R. Nix and A. J. Sierk, *Nucl. Phys. A* 489, 252 (1988).
8. J. Weber, H. C. Britt, A. Gavron, E. Konecky and J. B. Wilhelmy, *Phys. Rev. C* 13, 2413 (1976)
9. K.-H. Schmidt et al., *Nucl. Phys. A* 685, 60c (2001) *Phys. Rev. C* 13, 2413 (1976)
10. T. R. England and B. F. Rider, LA-UR 94-3106, ENDF-349 (1994)
11. F. J. Hambsch and S. Oberstedt, *Nucl. Phys. A* 617, 347 (1997)
12. M. Warda, K. Pomorski, J. L. Egido and L. M. Robledo, submitted to *J. Phys. G*
13. K. F. Flynn et al., *Phys. Rev. C* 5, 1725 (1972)
14. D. C. Hoffman et al., *Phys. Rev. C* 21, 972 (1980)
15. E. K. Hulet et al., *Phys. Rev. C* 40, 770 (1989)
16. M. Warda, J. L. Egido, L. M. Robledo and K. Pomorski, *Phys. Rev. C* 66, 014310 (2002)
17. P. Möller, D. G. Madland, A. J. Sierk and A. Iwamoto, *Nature (London)* 409, 785 (2001).
18. P. Möller, A. J. Sierk, T. Ichikawa and A. Iwamoto, *Prog. Th. Phys.* Suppl. 154, 21 (2004)
19. A. Dobrowolski, K. Pomorski and J. Bartel, *Nucl. Phys.* A729, 713 (2003)
20. R. Bass, *Nuclear Reactions with Heavy Ions* (Springer Verlag, Berlin, 1980)
21. S. Hofmann et al., *Z. Phys. A* 358, 377 (1997)